Science Advances
AAAS

advances.sciencemag.org/cgi/content/full/6/37/eabc0711/DC1

Supplementary Materials for

Mid-infrared polarization-controlled broadband achromatic metadevice

Kai Ou, Feilong Yu, Guanhai Li*, Wenjuan Wang, Andrey E. Miroshnichenko*, Lujun Huang, Peng Wang, Tianxin Li, Zhifeng Li, Xiaoshuang Chen*, Wei Lu

*Corresponding author. Email: ghli0120@mail.sitp.ac.cn (G.L.); andrey.miroshnichenko@unsw.edu.au (A.E.M.); xschen@mail.sitp.ac.cn (X.C.)

Published 11 September 2020, *Sci. Adv.* **6**, eabc0711 (2020)
DOI: 10.1126/sciadv.abc0711

The PDF file includes:

Other Supplementary Material for this manuscript includes the following:

(available at advances.sciencemag.org/cgi/content/full/6/37/eabc0711/DC1)

Supplementary Materials

Section S1. The design principle of all-Si broadband achromatic PCM and simulations for comparison between achromatic and chromatic PCMs.

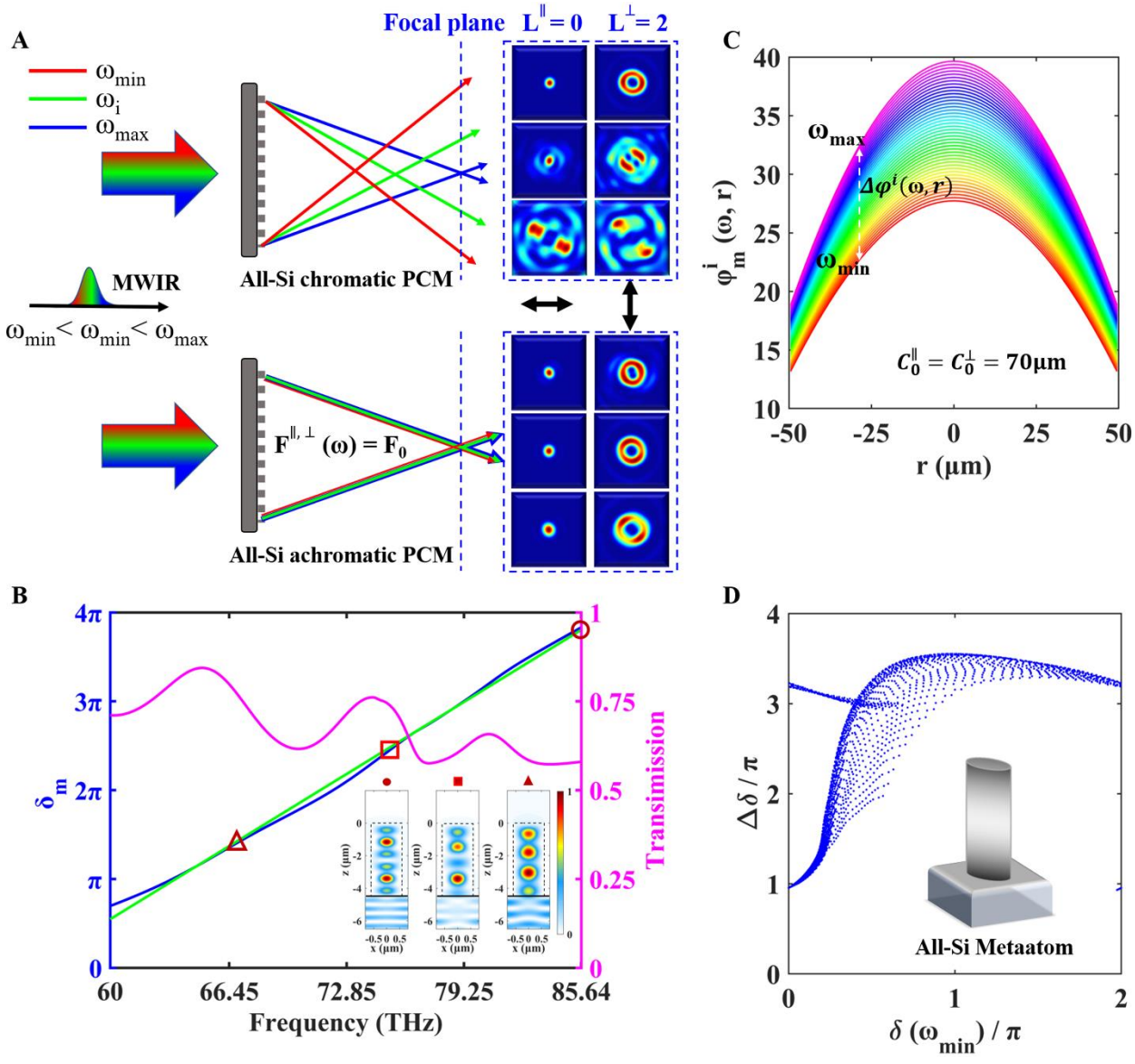

fig. S1. Comparisons between the metadevices without and with phase dispersion control and the design process of all-Si broadband achromatic polarization-controlled metadevices (PCMs) in MWIR. (A) Schematics for the focusing comparison of chromatic (top panel) and achromatic (bottom panel) PCMs. The insets

marking with blue dashed frame show the intensity profiles at the focal planes for wavelengths of 3.5μm, 4μm and 4.5μm from the top to bottom, respectively. Here, the focal plane intensity profiles are extracted from fig. S2 in which we design the chromatic and achromatic PCMs with $L^{\parallel} = 0$ and $L^{\perp} = 2$ for comparing their broadband performance with x- and y-polarized incidence. The left column corresponds to the x-polarization and the right for the y-polarization. **(B)** The transmission (pink solid line) and phase shift (blue solid line) spectra of the metaatom (Dx=1280nm, Dy=560nm) from 3.5 to 5μm. The green solid line is the linear fitting of the phase spectra for exacting the phase dispersion. The circle, square, and triangle symbols represent the phase shifts for different frequency points (λ=3.5μm, 4μm and 4.5μm), respectively. The insets are the corresponding magnetic energy density profiles along x-z cross-section (marking with the corresponding symbols). The black dashed line in the inset indicates the boundary of the nanostructure. **(C)** Required phase dispersion spectra to focus at designed wavelengths ranged from 3.5 to 5μm. **(D)** The phase-dispersion library. $\Delta\delta = \frac{d\delta}{d\omega}(\omega_{max} - \omega_{min})$ represent the dispersion of the metaatom (all-silicon elliptical nanopillar shown in the inset). $\delta(\omega_{min})$ is the phase shift of the lowest frequency.

Detailed design process for the broadband achromatic PCM

Fig. S1A schematically shows the focusing behaviors of chromatic (top panel) and broadband achromatic PCMs (bottom panel) when they are illuminated by a broadband MWIR light at normal incidence. In the case of the chromatic PCM, the intensity profiles at designed focal plane vary with incident wavelengths due to the wavelength dispersion determined by Eq. (1). The polarization-dependent focal spots for the monochromatic PCM show large distortions when operating wavelength is away from the designed λ=3.5μm. Compared with the chromatic PCM, the achromatic PCM shows excellent broadband achromatic performance. The focal length is unchanged with different incident wavelengths. The polarization-dependent focal spots show highly symmetric converging profiles (solid spots with L= 0 for x-polarization and doughnut-shaped ones with L= 2 for y-polarization) over the designed bandwidth.

Generally, the key point to realize broadband achromatism is to elaborately engineer and manipulate the phase dispersion of the building metaatoms, including the resonant phase dispersion of the metaatom and the intrinsic dispersion of the materials with which the metaatoms are made of. The intrinsic phase dispersion of the metaatoms leads to the wavelength dispersion and worsens the performance at the focal planes for monochromatic metadevice. For our all-silicon platform, the resonant phase dispersion plays a fundamental role in the achromatic design. It can be considered as wavelength-dependent resonant guide modes which result in different phase shifts with various frequencies for a given metaatom (see the inset in fig. S1B). As we have proved in the main text, the birefringent configuration of the metasurface allows us independently and efficiently tailoring the phase and phase dispersion for the orthogonal linear polarizations at subwavelength scale. To achieve the broadband performance, simultaneous control of the polarization-dependent phase shift (δ) and phase dispersion ($\frac{d\delta}{d\omega}$) imposed by the birefringent metaatoms is required.

Regarding this, the realization of the broadband performance of the PCM is turned to construct the mapping between the phase-dispersion spectrum (shown in Fig. 1C in main text and figs. S1B and S1D) imposed by each metaatom of the metadevices and the required phase shifts (shown in fig. S1C) at each frequency point within the designed bandwidth. In our work, the performances of the broadband multifunctional PCM follow Eq. (S1) (shown in fig. S1C). To achromatically manipulate the broadband incidence, the parameters should be dispersionless ($\frac{F^{\parallel,\perp}(\omega)}{d\omega} = 0, \frac{\Theta^{\parallel,\perp}(\omega)}{d\omega} = 0$). The phase spectra of the metadevices for each polarization state can be expressed as:

$$\varphi_m^i(r,\omega) = \frac{\omega}{c}\left(-\left(\sqrt{r^2 + (F_0^i)^2} - F_0^i\right) + xsin\left(\Theta_0^i\right)\right) + L^i\theta + C^i(\omega), (i = \parallel, \perp) \quad \text{(S1)}$$

where c is the speed of the light in free space, x, r and θ are the Cartesian and polar coordinates at the metasurface devices, respectively. $C^{\parallel,\perp}(\omega)$ determine the reference phase at each frequency and provide an additional optimal freedom in the design of the broadband achromatic metadevices. The choice of $C^{\parallel,\perp}(\omega)$ depends on the dispersion of the metaatom from the database shown in Fig. 1C in the main text. Here, $C^{\parallel,\perp}(\omega) = C_0^{\parallel,\perp}\omega/c$ is an optimized choice because of the near-linear phase dispersion of the metaatom from the database (shown in fig. S1B). The optimal $C_0^{\parallel,\perp}$ guarantee that the phase-dispersion range provided by the metaatom library (shown in fig. S1D) can cover the required ones according to Eq. (S1). Finally, at each frequency point, we can obtain the mapping between the phase spectrum ($\delta_m^{\parallel,\perp}(\omega) = \delta_m^{\parallel,\perp}(\omega_{min}) + \Delta\delta_m^{\parallel,\perp}(\omega)$) imposed by the birefringent metaatom from the database and the polarization-dependent modulated phase spectrum ($\varphi_m^{\parallel,\perp}(\omega) = \varphi_m^{\parallel,\perp}(\omega_{min}, r) + \Delta\varphi_m^{\parallel,\perp}(\omega, r)$) at each pixel (x, y) of the metadevice. With this mapping function, the broadband achromatic PCM for simultaneously engineering the polarization and dispersion can be achieved.

To clearly compare the broadband performance of the achromatic and chromatic PCMs, we have designed a polarization-selective BAFOV and chromatic PCM with diameters of 100μm. The chromatic metasurface is designed at the wavelength of 3.5μm. The specific parameters in Eq. (S1) are $\Theta_0^{\parallel,\perp} = 0$, $L^{\parallel} = 0$, $F_0^{\parallel} = 100\mu\text{m}$ and $L^{\perp} = 2$, $F_0^{\perp} = 100\mu\text{m}$. The simulations are shown in fig. S2. In this achromatic design, the optimal combination is $C_0^{\parallel} = C_0^{\perp} = 70\mu\text{m}$. The required phase dispersion spectrum is shown in fig. S1C. It can be seen that the achromatic PCM focuses the broadband light at the nearly same focal length and realizes the polarization-controlled beam generations shown in fig. S2A. However, the chromatic PCM shows strong dispersion behavior in the bandwidth. It has large focal length shifts and the dispersion significantly worsens its

performance when away from the designed wavelength (shown in fig. S2B). The results further confirm the validity of our broadband achromatic design with all-silicon platform.

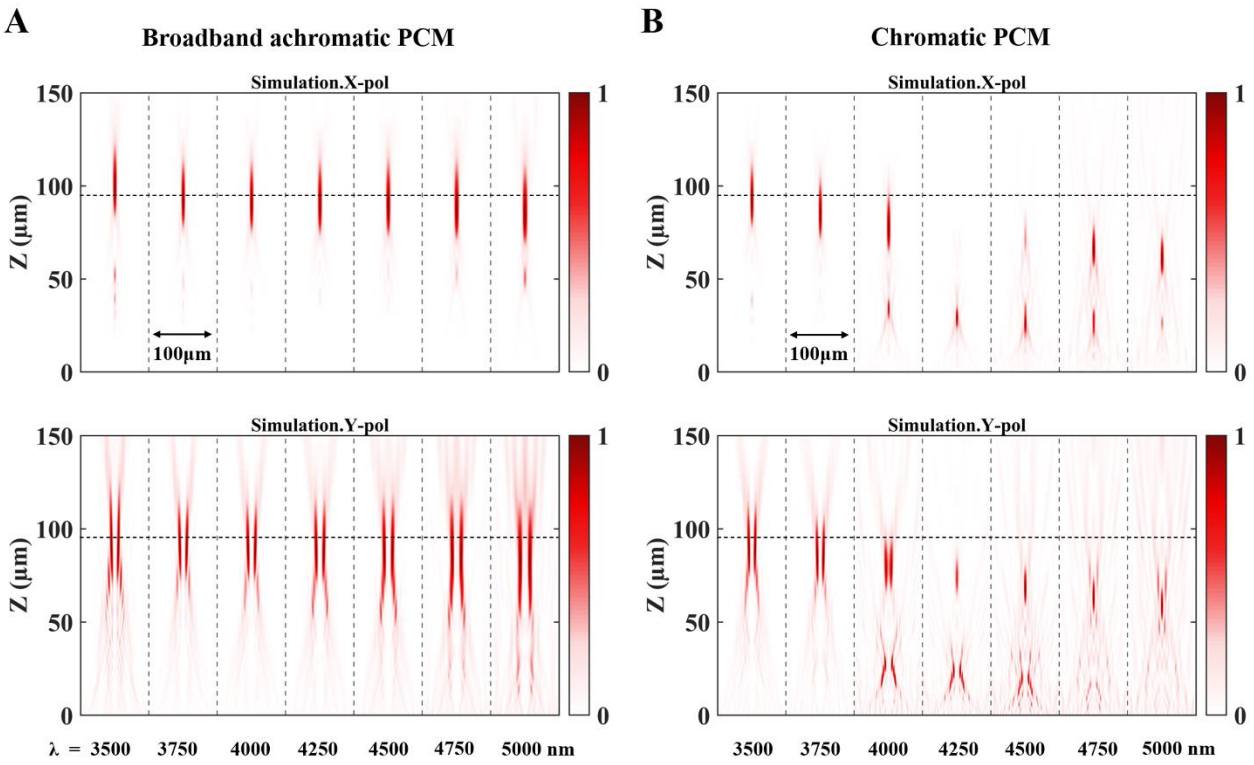

fig. S2. Simulated results for achromatic and chromatic PCMs (polarization-selective FOV generators) with x- and y-polarized incidence over the designed broad bandwidth from 3.5 to 5μm. (A) Intensity distribution profiles along x-z cross section for the incident light for the achromatic PCM. Top panel is for x-polarization and the bottom is for y-polarization. **(B)** Intensity distribution profiles along x-z cross-section for the chromatic PCM working at designed wavelength of 3.5μm. The black dashed lines represent the position of the focal planes. We can see that the broadband achromatic focusing behavior in **(A)** reveals the very well broadband performance in terms of wavefront modulation and polarization control.

Section S2. Scanning microscope imaging of the BAFS.

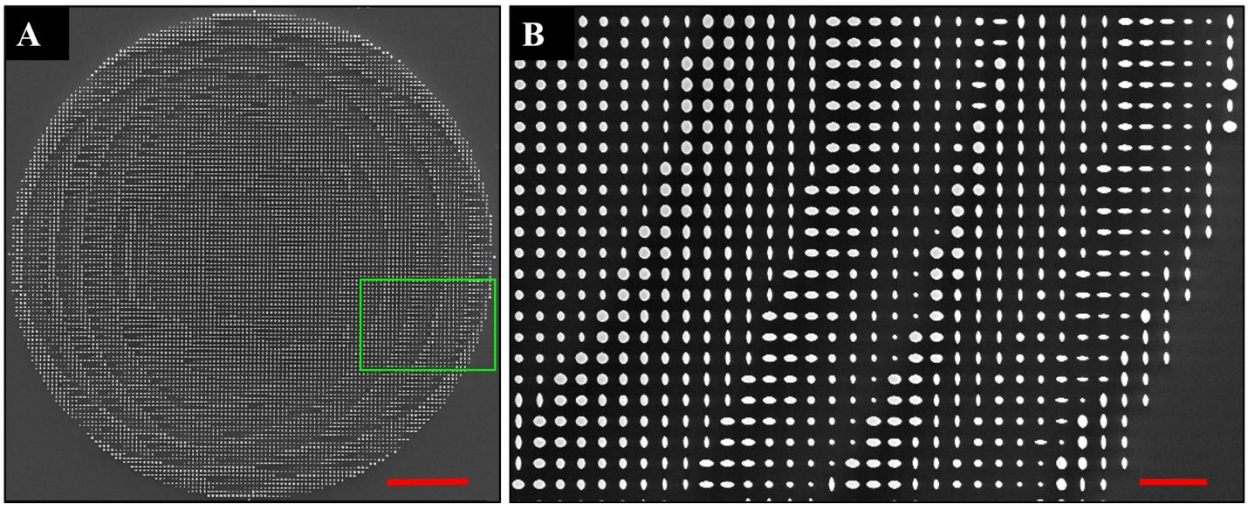

fig. S3. Scanning electron microscope images of the fabricated BAFS. (a) The overall SEM image of the BAFS. Scale bar is 18μm. **(b)** Top view of part of the sample marking with the green frame shown in (a). Scale bar, 5μm.

Section S3. Simulated results for the polarization-selective BAFOV and BAFS.

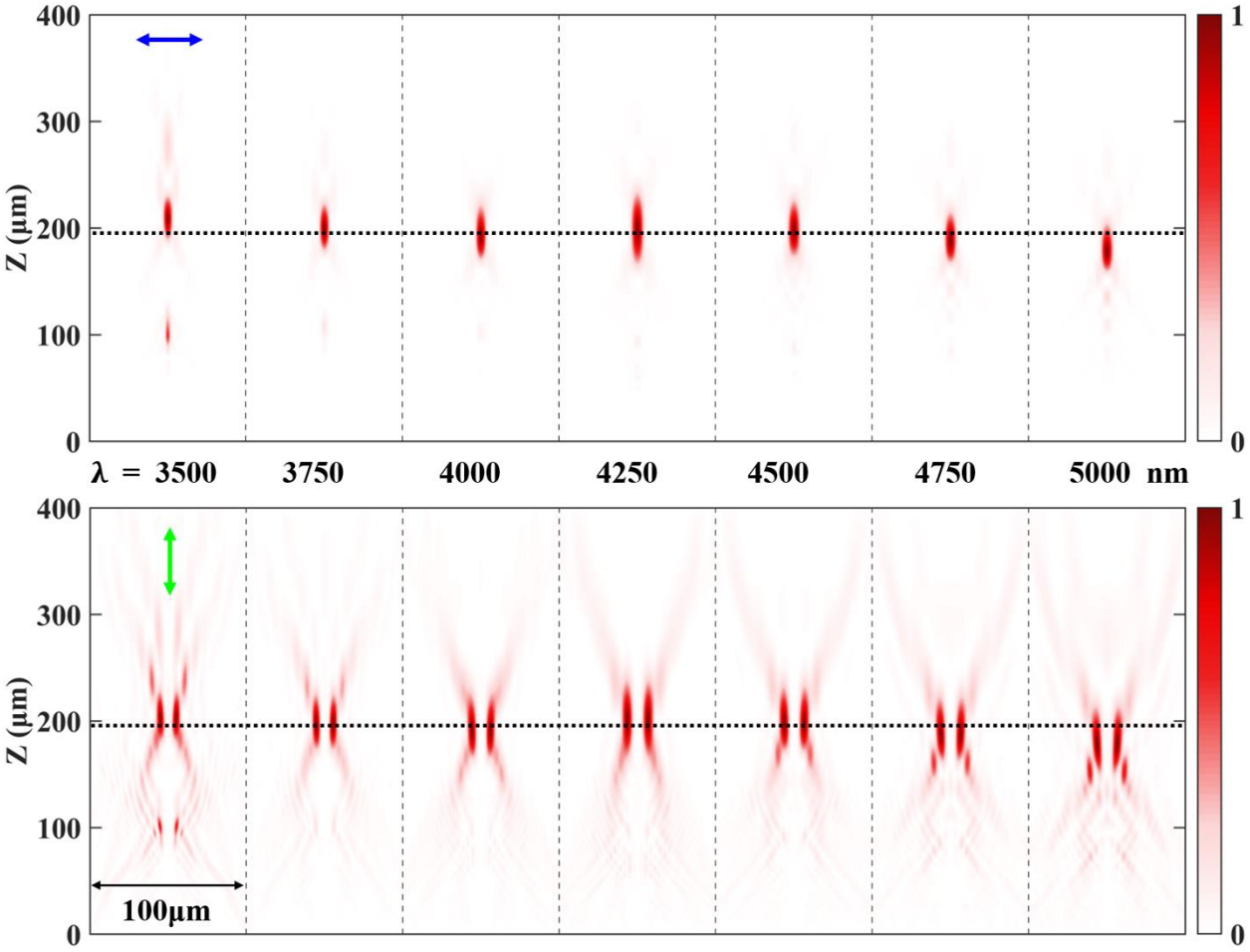

fig. S4. Simulated intensity distribution profiles along x-z cross-section over the designed wavelengths ranged from 3.5 to 5μm for the polarization-controlled BAFOV generator.

The top panel is for the x-polarized incidence and the bottom panel is for the y-polarization. The focal lengths show small variations from 1% to 6.5% relative to the mean focal length (indicated with the black dashed lines) over the entire designed wavelength range from 3.5 to 5μm. The results numerically prove the realization of the broadband achromatic focusing performance with polarization control.

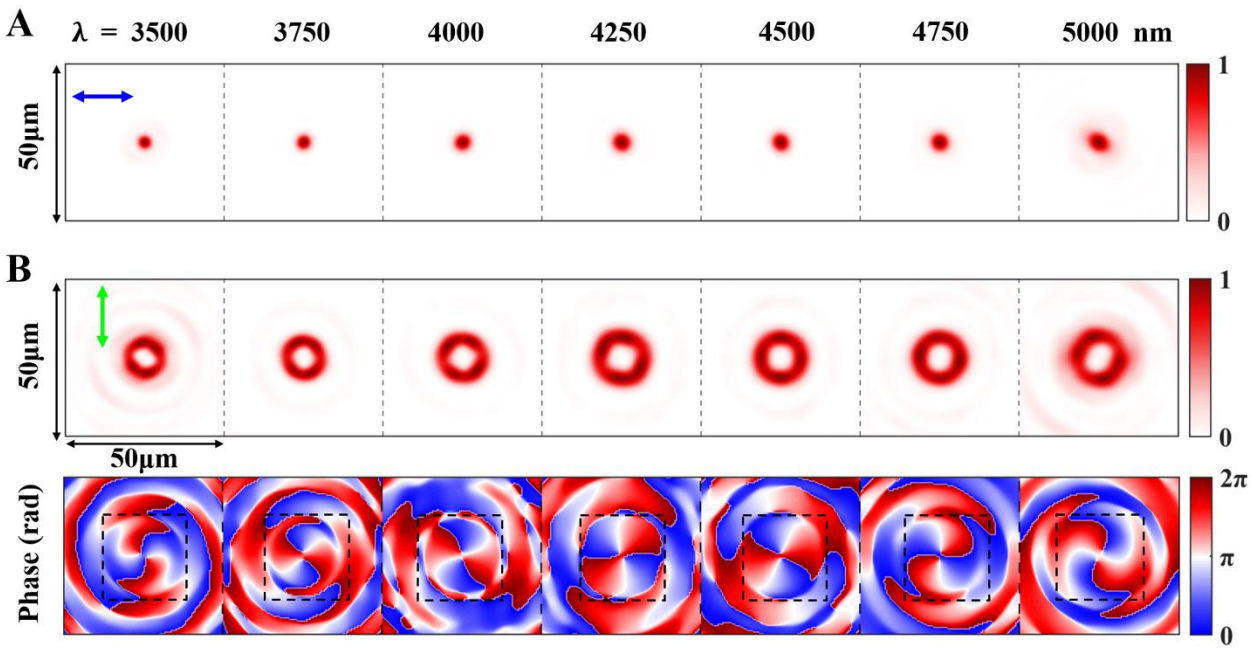

fig. S5. The transverse (x-y cross-section) intensity and phase profiles at the focal plane along the dashed line shown in fig. S4. (a) Simulations for the x-polarized incidence. The solid focal spots reveal that the focused beams are with topological charge number l=0. (**b)** Simulations for the y-polarized incident light. Top panel shows the intensity distributions and bottom panel demonstrates the corresponding phase profiles (the phase profiles of the focal spots marking with the black frame), which prove the realization of the BAFOV with the topological charge l=2. The results further confirm the polarization-controlled excellent behavior of the BAFOV generator.

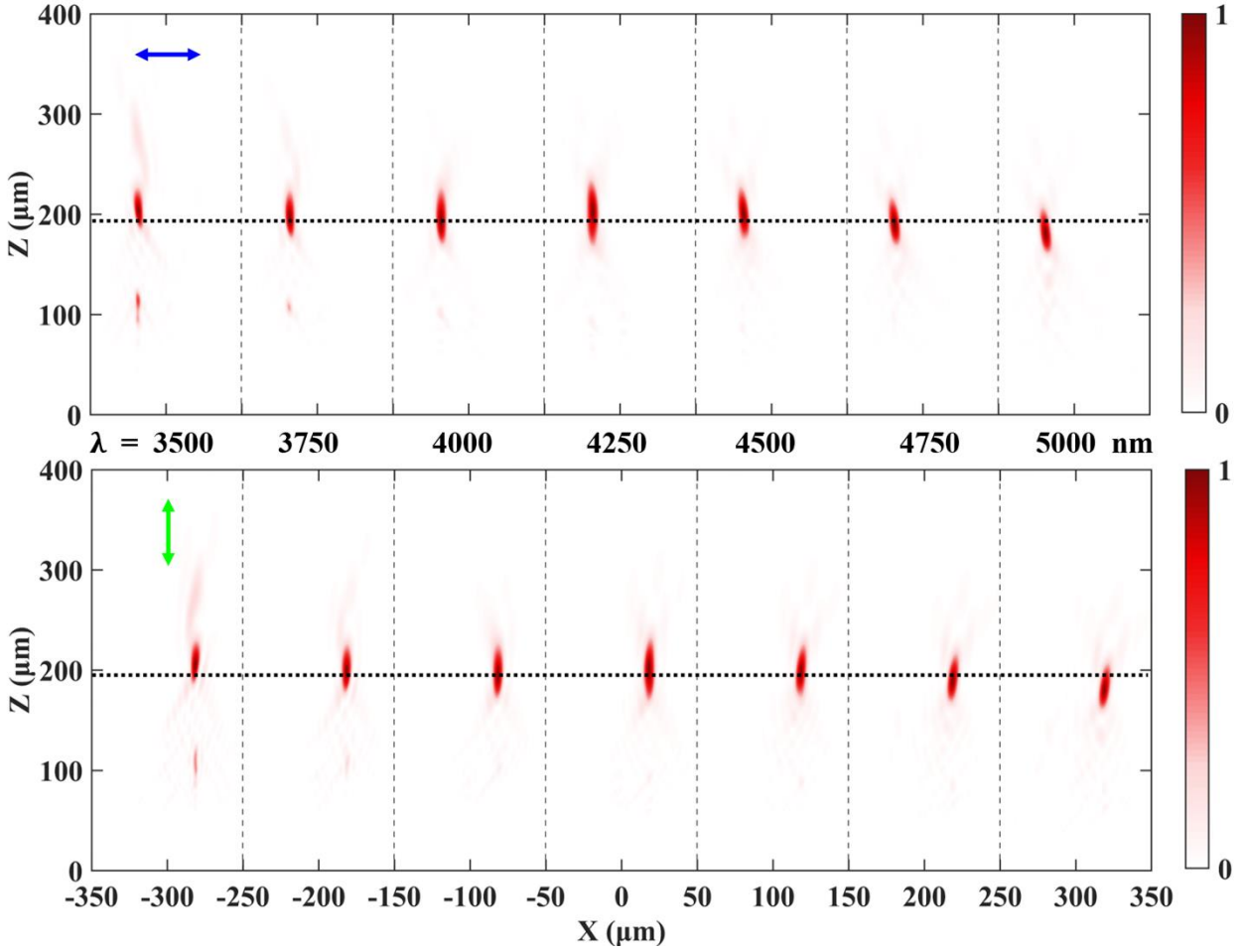

fig. S6. Simulated intensity profiles of x-z cross-section for the BAFS within the designed broadband bandwidth ranged from 3.5 to 5μm. The top panel is for x-polarized incidence and bottom panel is for y-polarization. The dotted line indicates the mean focal length over the entire designed wavelength range.

The small variations of the focal length (from 1.5% to 6.5% relative to the mean focal length over the entire designed wavelength ranged from 3.5 to 5μm) and the polarization-selective focal spot numerically proves the realization of polarization-controlled broadband achromatic focusing beam splitter (detailed discussions shown in main text).

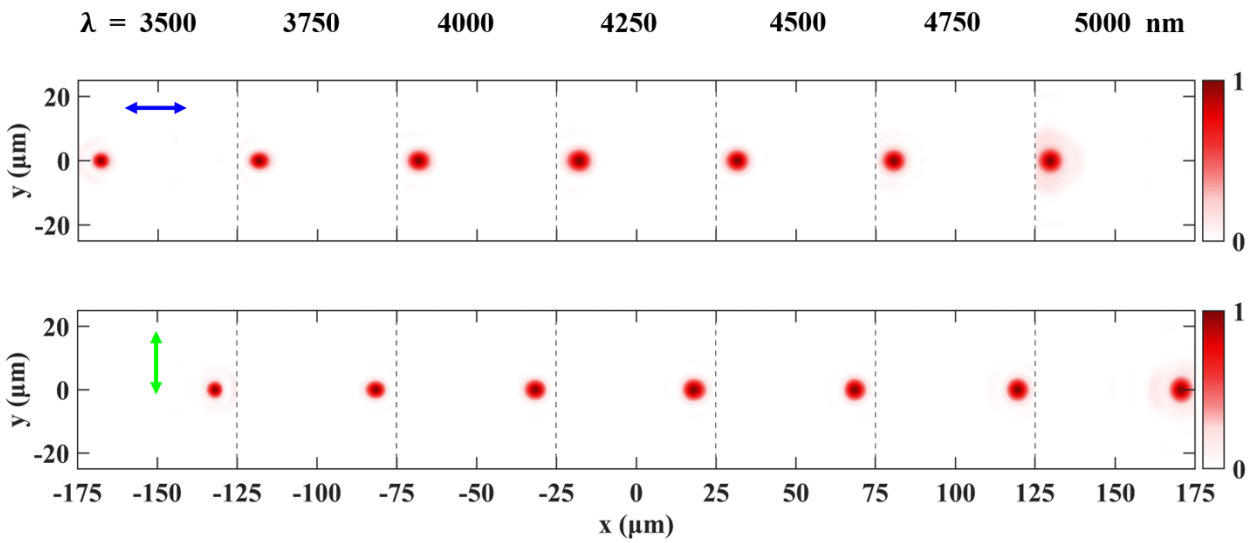

fig. S7. The corresponding focal plane intensity profiles along the black dotted line shown in fig. S6. The top and bottom panel is for x- and y-polarized incidence, respectively.

Movies S1 to S6